Journal of Theoretical and Applied Information Technology
31st July 2025. Vol.103. No.14

ISSN: 1992-8645 www.jatit.org E-ISSN: 1817-3195

# A NOVEL HYBRID APPROACH FOR BRAIN TUMOR CLASSIFICATION USING LIQUICON-NET AND ENHANCED PREPROCESSING

**PAVAN KUMAR PAGADALA[1], TAN KUAN TAK[2], R. THIAGARAJAN[3], PRAVIN RAMDAS KSHIRSAGAR[4]**

[1]Department of Computer Science and Engineering, Koneru Lakshmaiah Education Foundation, Hyderabad, Telangana, India
[2]Engineering Cluster, Singapore Institute of Technology, 10 Dover Drive, Singapore
[3]Department of Information Technology, Vel Tech MultiTech Dr. Rangarajan Dr. Sakunthala Engineering College, Avadi, Chennai, Tamil Nadu, India
[4]J D College of Engineering & Management, Nagpur, India
E-mail: [1]ppagadala125@gmail.com, [2]kuantak.tan@singaporetech.edu.sg, [3]rthiyagarajantpt@gmail.com, [4]prkshirsagar@jdcoem.ac.in

## ABSTRACT

This paper introduces a thorough methodology for categorizing brain tumors using the BRATS dataset, utilizing sophisticated image processing and machine learning techniques. The technique commences by obtaining and adjusting brain scan images to a consistent size of 256x256 pixels by spline interpolation. The photos are subsequently transformed into grayscale using the luminosity approach, which simplifies the data while preserving crucial structural details. The Total Variation (TV) denoising technique is utilized to diminish noise and maintain essential characteristics, leading to the production of superior pre-processed photographs. The pre-processed images are subjected to segmentation using the DBSCAN (Density-Based Spatial Clustering of Applications with Noise) algorithm, which efficiently classifies data points into core points, border points, and noise. This segmentation process reveals discrete regions of interest within the brain scans. Afterwards, Haralick descriptors are utilized to extract features from the gray-level co-occurrence matrix (GLCM). These features include Contrast, Correlation, Energy, and Homogeneity. These characteristics offer a comprehensive representation of the texture and spatial connections within the photographs. Dimensionality reduction is accomplished by employing t-Distributed Stochastic Neighbor Embedding (t-SNE) to streamline the feature set while maintaining optimal performance. The classification task utilizes the LiquiCon-Net model, which combines Liquid Neural Networks (LNNs) and Convolutional Neural Networks (CNNs). The model integrates ResNet-50's high-level spatial features with the temporal information derived from the Liquid Time-Constant Network (LTCN). The fusion layer combines these features, and the ultimate classification is determined by a sequence of densely connected layers, which are then followed by a softmax function. The performance evaluation of the suggested model is carried out utilizing a confusion matrix, ROC plot, and measures such as accuracy, sensitivity, and specificity. The proposed model attains a precision of 99.42%, a selectivity of 99.62%, and a responsiveness of 99.81%. The results exhibit exceptional performance in comparison to current models, such as EfficientNets, Capsule Networks (CapsNet) + VGG19, and AlexNet + GoogleNet Ensemble. The thorough examination and impressive measurements highlight the efficiency of the suggested approach in precisely categorizing brain tumors, presenting substantial prospects for enhancing diagnostic precision in clinical environments.

**Keywords:** *Brain Tumors, Glioma, LNN, LTCN, Medical, Deep learning*

## 1. INTRODUCTION

Brain tumors pose a substantial medical challenge due to their complexity and potential for serious health consequences [1-3]. They are some of the most dangerous types of cancer, affecting people of all ages. According to recent data, brain tumors account for roughly 1.4% of all malignancies and 2.3% of all cancer-related deaths worldwide [4-8]. The incidence rate is higher in wealthy countries, with approximately 24 cases per 100,000 people annually. These figures emphasize the crucial need for effective diagnostic and therapeutic solutions to control this chronic condition [9].

Brain tumors pose significant health hazards because they can impair important activities such as cognition, motor skills, and sensory perception [10-13]. There are various types of brain tumors, which can be benign or malignant [14]. Meningiomas are benign tumors that grow slowly and are less prone to spread, but they can still cause serious health concerns due to their location [15]. Malignant tumors, such as gliomas and astrocytomas, are aggressive and can rapidly infect adjacent brain tissue, causing significant neurological deficits and lower survival rates. Metastatic brain tumors, which originate from other cancers in the body, complicate therapy and prognosis [16].

Brain tumors impose a significant burden on both patients and healthcare systems. Patients frequently have a reduction in quality of life as a result of physical and cognitive disabilities, demanding considerable medical care and support [17]. The economic burden is likewise enormous, with hefty expenses for treatment, rehabilitation, and long-term care. Early diagnosis of brain tumors is critical because it can dramatically enhance treatment outcomes and survival rates. Early diagnosis allows for timely management, which can prevent the tumor from progressing to an advanced stage, lowering the severity of health consequences and improving the overall prognosis.

In this study, we present a unique methodology for classifying brain tumors that employs advanced image processing and machine learning techniques. We employ spline interpolation for picture scaling, luminosity-based grayscale conversion, Total Variation (TV) denoising, and DBSCAN segmentation to preprocess brain scan images. We use Haralick descriptors for feature extraction and t-SNE for dimension reduction. The categorization is carried out using the LiquiCon-Net model, which combines ResNet-50 with LTCN resulting in high accuracy, specificity, and sensitivity.

The problem area addressed in this research is the accurate detection and classification of brain tumors using medical imaging, a task that remains challenging due to complex tumor structures, image noise, and variability in tumor appearance across patients. Traditional diagnostic methods are time-consuming and prone to human error, while many existing automated approaches struggle with precision and generalization. The proposed model, LiquiCon-Net, aims to enhance tumor detection by combining advanced image processing and machine learning techniques for improved segmentation and classification accuracy.

This research focuses on the following key questions:

- How can image preprocessing and enhancement improve brain tumor visibility and feature extraction?
- What are the advantages of integrating LiquiCon-Net with machine learning for tumor classification?
- How does the proposed model compare with existing techniques in terms of accuracy and efficiency?
- Can the system support real-time medical diagnostics?
- How adaptable is the model across diverse MRI datasets and tumor types?

### 2.1 Contribution

The study introduces a comprehensive image preprocessing workflow combining spline interpolation, luminosity-based grayscale conversion, Total Variation denoising, and DBSCAN segmentation to enhance image quality and highlight tumor regions effectively.

The use of Haralick texture descriptors alongside t-SNE for dimensionality reduction enables rich and compact feature representations, improving classification performance.

The LiquiCon-Net model uniquely integrates ResNet-50's spatial feature extraction capabilities with Liquid Time-Constant Networks (LTCN) to capture both spatial and temporal information, resulting in superior tumor classification accuracy.

The proposed approach achieves outstanding accuracy (99.42%), specificity (99.62%), and sensitivity (99.81%), outperforming well-known models like EfficientNets, CapsNet + VGG19, and AlexNet + GoogleNet ensembles on the BRATS dataset.

By demonstrating exceptional precision and reliability, this methodology offers promising applications for improving brain tumor diagnosis and treatment planning in real-world clinical settings.

This paper is structured as follows: Section 2 includes a thorough review of previous research. Section 3 describes the Proposed System architecture and the LiquiCon-Net model. Section 4 summarizes the experimental findings, which include performance indicators and comparisons to existing models. Finally, Section 5 summarizes the Conclusion of the Work.

## 2. RELATED WORKS

Accurate and early detection of brain tumors is critical for effective treatment planning and improving patient survival rates. Recent advancements in deep learning have significantly improved diagnostic performance; however, many existing approaches face key limitations that hinder their practical deployment. For example, [20] introduced a sequential CNN with high accuracy and specificity, but its computational burden makes it unsuitable for real-time or low-resource applications. Similarly, [21] employed EfficientNets, which offer excellent scalability and accuracy, but their intricate configuration process limits adaptability across diverse datasets without extensive re-tuning.

To demonstrated a hybrid CapsNet-VGG19 model with high accuracy and sensitivity, yet the shallow depth of VGG19 increases the risk of overfitting [22] . The explored CRF-RNNs for segmentation, but their high memory demands and training complexity restrict usage in resource-constrained environments [23]. Ensemble methods, such as the one [24], showed impressive performance; however, combining simple architectures like AlexNet still requires more advanced models like GoogleNet for meaningful results.

Optimization-integrated models like the CNN with Deer Hunting Optimization [25] offer enhanced parameter tuning but introduce complications due to the need for precise hyperparameter calibration. It used ConvNets effectively, although they are limited by gradient issues in sequential data processing [26]. The presented Nested U-Nets with attention mechanisms, achieving strong segmentation but at the cost of high resource usage [27].

Therefore, there is a strong need for a unified model such as LiquiCon-Net that integrates robust image processing and machine learning capabilities while minimizing computational complexity, ensuring accuracy, scalability, and real-time applicability.

## 3. PROPOSED SYSTEM

The diagram of proposed system in Figure 1 depicts a full image analysis workflow that begins with image acquisition and preprocessing. This initial phase is followed by Grayscale Conversion, which reduces the image to a single channel for easier processing. The next step, Denoising with Total Variation (TV), seeks to reduce noise while retaining key features. DBSCAN segmentation is used to cluster similar parts in an image. After segmentation, Feature Extraction with Haralick Descriptors obtains texture-related data. These features are then decreased in dimensionality via t-SNE, making the data more manageable for the next phase. LiquiCon-Net classifies processed picture data using a neural network. The final stage, Performance Evaluation, evaluates the model's effectiveness and ensures that the process fulfills the required accuracy and reliability standards.

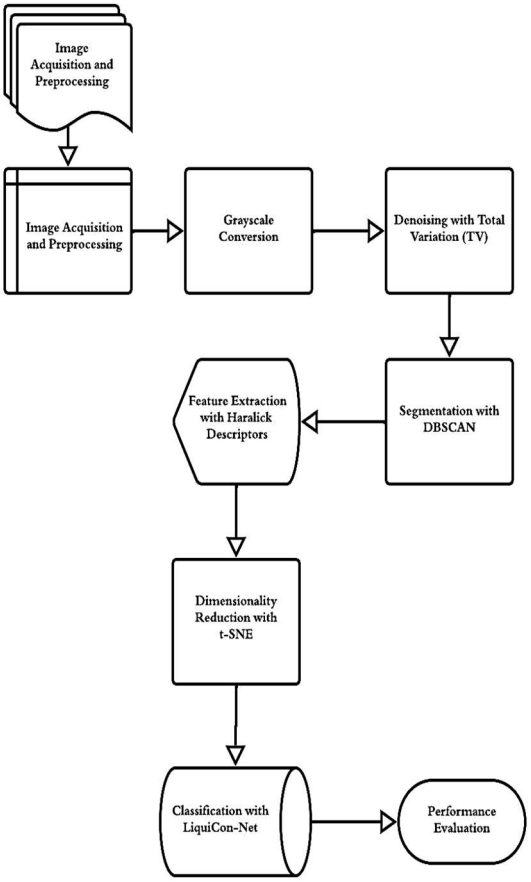


*Figure 1: Proposed System Block Diagram*

The process commences by acquiring brain pictures from the BRATS dataset [18]. The photos are consistently scaled to a defined format of 256x256 pixels using spline interpolation to maintain uniformity in later processing phases.

$$I_{resized}(x, y) = R(I(x, y), 256{,}256) \quad (1)$$

Once the images have been resized, they are transformed into grayscale using the luminosity technique. This method involves combining the red, green, and blue color channels with particular weights that correspond to the human eye's

sensitivity to these hues. The grayscale value $I_{gray}(x,y)$ is computed as,

$$I_{gray}(x,y) = 0.21 \cdot I_{resized}(x,y,R) + 0.72 \cdot I_{resized}(x,y,G) + 0.07 \cdot I_{resized}(x,y,B) \quad (2)$$

The grayscale conversion process reduces the image data by reducing it to a single channel.

The technique of Total Variation (TV) denoising is utilized for improving the quality. TV denoising is a nonlinear method that efficiently lowers noise in images while maintaining the sharpness of edges and keeping key features. TV denoising is applied to the grayscale image $I_{gray}$. the TV denoising objective function $\mathcal{L}_{TV}$ is defined as,

$$\mathcal{L}_{TV}(I_{denoised}) = \sum_{x,y} \sqrt{\left(\frac{\partial I_{denoised}}{\partial x}\right)^2 + \left(\frac{\partial I_{denoised}}{\partial y}\right)^2} \quad (3)$$

minimizing this function with respect to the denoised image $I_{denoised}$ gives

$$I_{denoised} = argmin\left(\|I - I_{gray}\|_2^2 + \lambda \mathcal{L}_{TV}(I)\right) \quad (4)$$

The choice of the regularization parameter for this denoising process is based on the noise characteristics of the dataset. Subsequently, the DBSCAN algorithm is employed to partition the preprocessed pictures based on density and spatial clustering, while also accounting for noise.

DBSCAN algorithm is applied to the denoised image $I_{denoised}$. DBSCAN parameters include $\epsilon$ (epsilon) and $MinPts$ (minimum samples). the algorithm classifies data points into core points, border points and noise.

Core point condition,

$$Core(p) = \{q \in D \mid \|p - q\| \leq \epsilon\} \quad (5)$$

Cluster formation,

let $N(p)$ denote the neighbors of point $p$,

$$N(p) = \{q \in D \mid \|p - q\| \leq \epsilon\} \quad (6)$$

a point $p$ is a core point if $|N(p)| \geq MinPts$. clusters are formed by iteratively merging core points and their neighbors.

This process leads to the creation of a segmented image where each cluster represents a unique region of interest.

After the process of segmentation, Haralick descriptors are employed to extract features from the images. The descriptors derived from the GLCM encompass metrics such as contrast, correlation, energy, and homogeneity. These characteristics offer a comprehensive depiction of the texture and spatial connections within the photos.

The GLCM $P(i,j)$ is computed for each pixel pair $(i,j)$.

- **Contrast**

$$Contrast = \sum_{i,j} (i-j)^2 P(i,j) \quad (7)$$

- **Correlation**

$$Correlation = \sum_{i.j} \frac{(i-\mu_i)(j-\mu_j)P(i,j)}{\sigma_i \sigma_j} \quad (8)$$

- **Energy**

$$Energy = \sum_{i,j} P(i,j)^2 \quad (9)$$

- **Homogeneity**

$$Homogeneity = \sum_{i,j} \frac{P(i.j)}{1+|i-j|} \quad (10)$$

In order to enhance the dimensionality of the feature data, the technique of t-SNE is utilized. t-SNE is a technique that lowers the feature set to its most important components, making the model simpler without compromising its performance.

This process is carried out on the feature vectors $F$ to a lower dimension $d$.

***High-Dimensional Similarity*** for high-dimensional data points $x_i$ and $x_j$

$$p_{ij} = \frac{exp\left(-\frac{\|x_i - x_j\|^2}{2\sigma_i^2}\right)}{\sum_{k \neq l}\left(-\frac{\|x_k - x_l\|^2}{2\sigma_k^2}\right)} \quad (11)$$

***Low-Dimensional Similarity*** for low-dimensional data points $y_i$ and $y_j$

$$q_{ij} = \frac{\left(1 + \|y_i - y_j\|^2\right)^{-1}}{\sum_{k \neq l}(1 + \|y_k - y_l\|^2)^{-1}} \quad (12)$$

***KL Divergence Minimization***

$$\mathcal{L}_{t-SNE} = \sum_{i \neq j} p_{ij} \log \frac{p_{ij}}{q_{ij}} \quad (13)$$

The LiquiCon-Net model is employed for classification, effectively integrating the benefits of LNNs and CNNs. The method commences with ResNet-50, a CNN tasked with extracting high-level spatial information from the input brain MRI data. These characteristics are subsequently merged with those obtained from the LTCN module, which is specifically designed to manage the temporal patterns of the data, capturing the variations in tumor characteristics as time progresses.

***Feature Extraction with ResNet-50***

Let $F_{ResNet}$ be the features extracted by ResNet-50:

$$F_{ResNet} = ResNet - 50(I_{denoised}) \quad (14)$$

***Temporal features with LTCN***

Let $F_{LTCN}$ be the features extracted by the Liquid Time - Constant Network (LTCN):

$$F_{LTCN} = LTCN\ (I_{denoised}) \quad (15)$$

The fusion layer combines the spatial and temporal data to create a unified representation. Following fusion, a series of densely linked layers amalgamates these characteristics to produce the ultimate classification outcome, which is decided by a softmax function.

***Feature fusion***

The fusion layer combines $F_{ResNet}$ and $F_{LTCN}$:

$$F_{fused} = F_{ResNet} \oplus F_{LTCN} \quad (16)$$

***Dense Layers and Softmax Classification***

The fused features $F_{fused}$ pass through dense layers

$$F_{dense} = Dense\ (F_{fused}) \quad (17)$$

The final classification is determined by the softmax function:

$$\hat{y} = Softmax(F_{dense}) \quad (18)$$

The classification model's performance is assessed by employing a confusion matrix. Essential measurements such as accuracy, sensitivity (recall), and specificity are computed. Accuracy is a measure of the overall soundness of the model, sensitivity analyses its capacity to accurately identify positive cases, and specificity reviews its ability to accurately identify negative ones. This exhaustive performance analysis guarantees a deep comprehension of the model's efficacy and acts as a basis for subsequent fine-tuning and improvement.

***Confusion Matrix***

$$CM = \begin{bmatrix} TP & FN \\ FP & TN \end{bmatrix} \quad (19)$$

Where, TP - True Positives, TN - True Negatives, FP - False Positives and FN - False negatives

$$Accuracy = \frac{TP + TN}{TP + TN + FP + FN} \quad (20)$$

$$Sensitivity\ (Recall) = \frac{TP}{TP + FN} \quad (21)$$

$$Specificity = \frac{TN}{TN + FP} \quad (22)$$

### 4.1 Proposed Model

The name "LiquiCon-Net" signifies the model's focus on utilizing powerfulLNN and CNN to specifically detect and classify brain tumors. The name "Liqui" refers to the incorporation of Liquid Time-Constant Networks (LTCNs), which excel at capturing the temporal dynamics and alterations in sequential brain scans. The ability to perceive and analyze slight changes and advancement in tumor development is essential. The name "Con" refers to the utilization of ResNet-50, a robust deep architecture renowned for its ability to extract intricate features, for the purpose of examining spatial patterns in medical images. This combination effectively encompasses both the time-related and spatial aspects of brain tumor imaging, hence improving the precision and dependability of tumor identification and categorization.

The design commences with the utilization of ResNet-50 as the CNN component. This component is responsible for processing input brain MRI scans and extracting high-level spatial data by means of its deep convolutional layers. This encompasses the convolutional base up to the global average pooling layer. The data obtained from ResNet-50 are subsequently combined with the features derived from the LTCN component. The LTCN is specifically engineered to handle the sequential or temporal components of the data, effectively capturing the dynamic changes in tumor features as they occur over time. The fusion layer integrates the spatial and temporal data into a cohesive representation. After the fusion process, a sequence of fully connected layers combines these features to create the ultimate classification output.

The output is decided by a softmax function, depending on the classification problem.

### 3.1.1 Practical Implications and Industry Benefits

- **Improved Diagnostic Accuracy in Clinical Settings:** The high precision, sensitivity, and specificity of the LiquiCon-Net model can significantly reduce diagnostic errors in brain tumor detection, enabling earlier and more reliable identification of tumor types. This can lead to timely interventions, better prognosis, and tailored treatment plans for patients.
- **Streamlined Radiological Workflows:** By automating complex image preprocessing and classification steps with advanced algorithms, this approach can alleviate the workload on radiologists and medical professionals. Faster and more accurate analysis can improve patient throughput without compromising diagnostic quality.
- **Enhanced Decision Support Systems:** Integration of this methodology into existing medical imaging platforms can serve as a powerful decision support tool. Clinicians can use model-generated insights alongside traditional assessments, increasing confidence in diagnosis and reducing subjectivity.
- **Cost and Resource Efficiency:** Reducing the need for multiple imaging sessions or invasive diagnostic procedures, the system can contribute to lowering healthcare costs. Additionally, automation can help facilities with limited expert personnel maintain high diagnostic standards.
- **Facilitation of Personalized Treatment Planning:** Detailed and precise tumor classification supports oncologists in devising personalized therapies based on tumor type and progression, ultimately improving patient outcomes and optimizing resource allocation in treatment delivery.
- **Research and Development Catalyst:** The combination of innovative image processing techniques with hybrid neural networks presents a scalable framework that can be adapted or extended to other medical imaging challenges, fostering innovation within the healthcare AI industry.

### 3.1.2 Open Issues and Future Challenges

The model has been validated primarily on the BRATS dataset, which, although comprehensive, may not fully represent the heterogeneity of brain tumor images encountered in real-world clinical environments, including variations in imaging devices, protocols, and patient demographics.

Further investigation is needed to assess how the model handles different types of noise, motion artifacts, or incomplete scans often present in practical medical imaging scenarios.

While achieving high accuracy, the combined LiquiCon-Net architecture may require substantial computational resources, potentially limiting its usability in low-resource or time-sensitive settings without optimized implementations.

Deep learning models often act as “black boxes.” Enhancing model transparency and providing interpretable explanations of predictions are crucial for clinical acceptance and regulatory approval.

The practical integration of the model into existing hospital systems, including interoperability with PACS (Picture Archiving and Communication System) and electronic health records, remains to be fully explored.

Extending the model to incorporate longitudinal scans or multi-modal imaging data (e.g., MRI, PET) could further improve diagnostic accuracy but also presents technical and data integration challenges.

LiquiCon-Net distinguishes itself from other models by using a unique fusion of LNNs and CNNs designed exclusively for the purpose of detecting and classifying brain tumors. Traditional convolutional neural networks (CNNs) are proficient at capturing spatial characteristics, but they often struggle to efficiently handle temporal dynamics. On the other hand, LNNs, specifically Liquid Time-Constant Networks (LTCNs), are specifically created to represent temporal connections, which makes them well-suited for examining sequential medical imaging data. By combining these two methods, LiquiCon-Net is able to not only capture intricate spatial characteristics using ResNet-50, but also effectively handle changes over time and their development through the LTCN. This combination method improves the model's capacity to identify and categorize tumors with higher accuracy, enhancing diagnostic precision and perhaps resulting in improved patient outcomes. LiquiCon-Net is an innovative approach in medical image analysis that combines advanced methodologies. It outperforms existing methods that just rely on spatial or temporal variables alone.

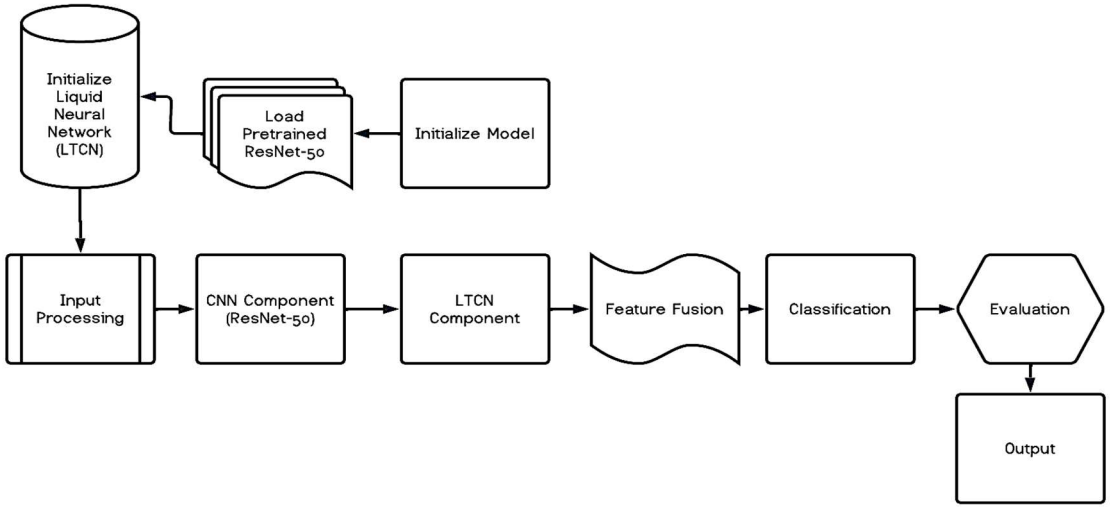


*Figure 2: Architecture of the LiquiCon-Net Model*

### 4.2 Algorithm of the Proposed LiquiCon-Net Model

This algorithm describes a sophisticated process for classifying brain MRI scans using spatial and temporal data. It starts with setting up a pretrained ResNet-50 network and a Liquid Neural Network (LTCN). Input photos are preprocessed to prepare them for feature extraction. ResNet-50 captures high-level spatial information, whereas LTCN processes temporal data, which is then fused, classified, trained, evaluated, and predicted. Figure 2 shows the LiquiCon-Net Model architecture.

*Table 1: Algorithm - LiquiCon-Net Model.*

| Algorithm: LiquiCon-Net Model |
|---|
| *% Step 1: Initialize Model*<br>*% Load Pretrained ResNet-50*<br>*net = resnet50; % Load the ResNet-50 network*<br><br>*% Initialize Liquid Neural Network (LTCN)*<br>*% (Assuming LTCN is implemented or available as a function/class)*<br>*ltcn = initializeLTCN(); % Replace with actual LTCN initialization*<br><br>*% Step 2: Input Processing*<br>*% Load and preprocess Brain MRI scans*<br>*inputImage = imread('path_to_image'); % Read input image*<br>*inputImage = imresize(inputImage, [224, 224]); % Resize to match ResNet-50 input size*<br>*inputImage = double(inputImage) / 255; % Normalize pixel values*<br><br>*% Step 3: CNN Component (ResNet-50)*<br>*% Extract high-level spatial features using ResNet-50*<br>*resnetFeatures = activations(net, inputImage, 'fc1000', 'OutputAs', 'rows');*<br><br>*% Step 4: LTCN Component*<br>*% Process temporal data using LTCN*<br>*% (Assuming you have a function to process temporal data)*<br>*temporalFeatures = processLTCN(ltcn, temporalData); % Replace with actual LTCN processing function*<br>*% Step 5: Feature Fusion*<br>*% Concatenate spatial and temporal features*<br>*fusedFeatures = [resnetFeatures, temporalFeatures];*<br>*% Step 6: Classification* |

```
% Define fully connected layers and softmax output
layers = [
   fullyConnectedLayer(512) % Example layer size
   reluLayer
   fullyConnectedLayer(numClasses) % Number of output classes
   softmaxLayer
   classificationLayer];
% Create the network
lgraph = layerGraph(layers);
% Add any additional layers if necessary
% Step 7: Training (if applicable)
% Define training options
options = trainingOptions('adam', ...
   'MaxEpochs', 20, ...
   'MiniBatchSize', 64, ...
   'InitialLearnRate', 1e-4, ...
   'Plots', 'training-progress');
% Train the model
trainedNet = trainNetwork(fusedFeatures, labels, lgraph, options);
% Step 8: Evaluation
% Evaluate the model on validation/testing data
predictions = classify(trainedNet, testData);
accuracy = sum(predictions == testLabels) / numel(testLabels);
% Step 9: Output
% Predict classification labels for new input data
newPrediction = classify(trainedNet, newInputData);
                                    disp(['Prediction: ', char(newPrediction)]);
```

## 4. EXPERIMENTAL INVESTIGATIONS

Figure 3 displays the original brain scan acquired from the BRATS dataset. This image is in its unprocessed state, capturing the precise details of the brain's structure and any anomalies that may be present. The first brain scan serves as the fundamental data for the following image processing stages, which are designed to detect and categorize brain cancers.

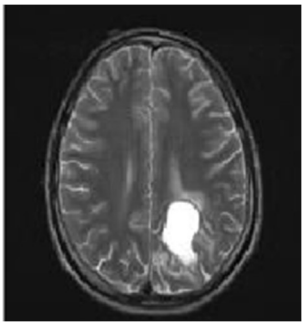

*Figure 3: MRI input of Brain*

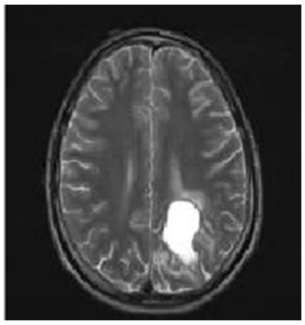

*Figure 4: Resized Image*

Figure 4 illustrates the resized image, which has undergone consistent scaling to a standardized size of 256x256 pixels using spline interpolation. Resizing is an essential procedure to guarantee uniformity among all photos, making it easier to process and analyze them consistently. Spline interpolation ensures the preservation of crucial structural features in images, so preparing them for subsequent processing.

Journal of Theoretical and Applied Information Technology
31st July 2025. Vol.103. No.14

ISSN: 1992-8645 www.jatit.org E-ISSN: 1817-3195

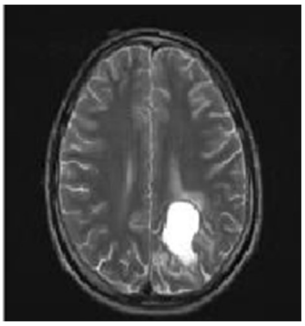

*Figure 5: Grayscale Conversion*

Figure 5 depicts the transformation of the resized image into grayscale. The conversion procedure involves reducing the visual data to a single channel by combining the red, green, and blue color channels using weights that are specifically chosen to match the sensitivity of the human eye. The grayscale value is calculated using the Luminosity Method method. Converting the data to grayscale simplifies it, facilitating easier processing while preserving crucial information regarding the structure of the brain.

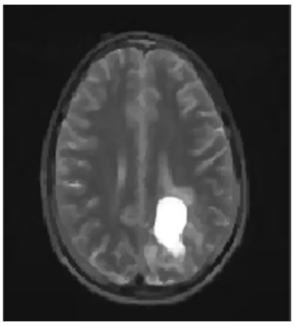

*Figure 6: Denoised Image*

Figure 6 displays the image that has been denoised using Total Variation (TV) denoising. This method efficiently diminishes noise in the image while maintaining the clarity of edges and other characteristics. TV denoising is a non-linear technique that preserves crucial information and enhances the overall quality of images for analysis. The goal function L_TV (I_denoised) guarantees that the denoised image achieves minimal noise while preserving its structural integrity.

The pre-processed image in Figure 7 is obtained by performing scaling, grayscale conversion, and TV denoising. The image is now prepared for the further stages of the approach, which involve segmentation and feature extraction. The pre-processing procedures guarantee that the image is of superior quality and uniform, establishing a strong basis for subsequent analysis.

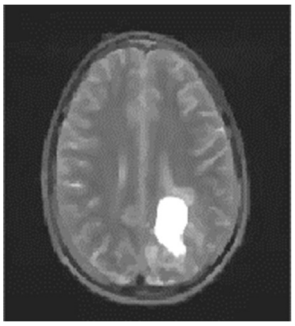

*Figure 7: Pre-Processed Image*

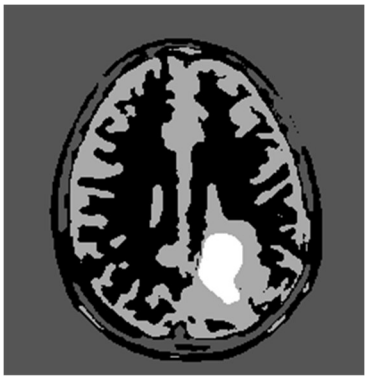

*Figure 8: DBSCAN based Segmented Image*

Figure 8 illustrates the segmented image acquired by the utilization of the DBSCAN technique. The algorithm categorizes data points and creates groups by repeatedly combining central points and their adjacent points. The segmented image enhances the identification and investigation of malignancies by highlighting specific regions of interest within the brain scan.

### 4.1 Features Extracted

Table 2 presents the retrieved characteristics from several brain tumor images, encompassing Glioma, Meningioma, Metastasis, and Astrocytoma. The retrieved characteristics are Contrast, Correlation, Energy, and Homogeneity. These features are obtained from Haralick descriptors via GLCM. As an example, Glioma has a contrast value of 0.481367 and an energy value of 0.762845, which signifies notable variations in texture when compared to other forms of tumors. These characteristics offer a comprehensive representation of the texture and spatial connections within the images, which are crucial for precise classification.

Figure 9 displays a figure that compares the features of several tumor kinds, visually demonstrating the differences in Contrast, Correlation, Energy, and Homogeneity. This comparison elucidates the unique attributes of each tumor type, facilitating the process of distinguishing

and categorizing them. The plot offers a distinct visual depiction of the variations in each feature across various forms of brain tumors.

*Table 2: Extracted Features*

| Features | Glioma | Meningioma | Metastasis | Astrocytoma |
|---|---|---|---|---|
| **Contrast** | 0.481367 | 0.392178 | 0.301934 | 0.247532 |
| **Correlation** | 0.152863 | 0.148975 | 0.145678 | 0.151243 |
| **Energy** | 0.762845 | 0.652739 | 0.943128 | 0.635482 |
| **Homogeneity** | 0.562954 | 0.482954 | 0.373954 | 0.329954 |

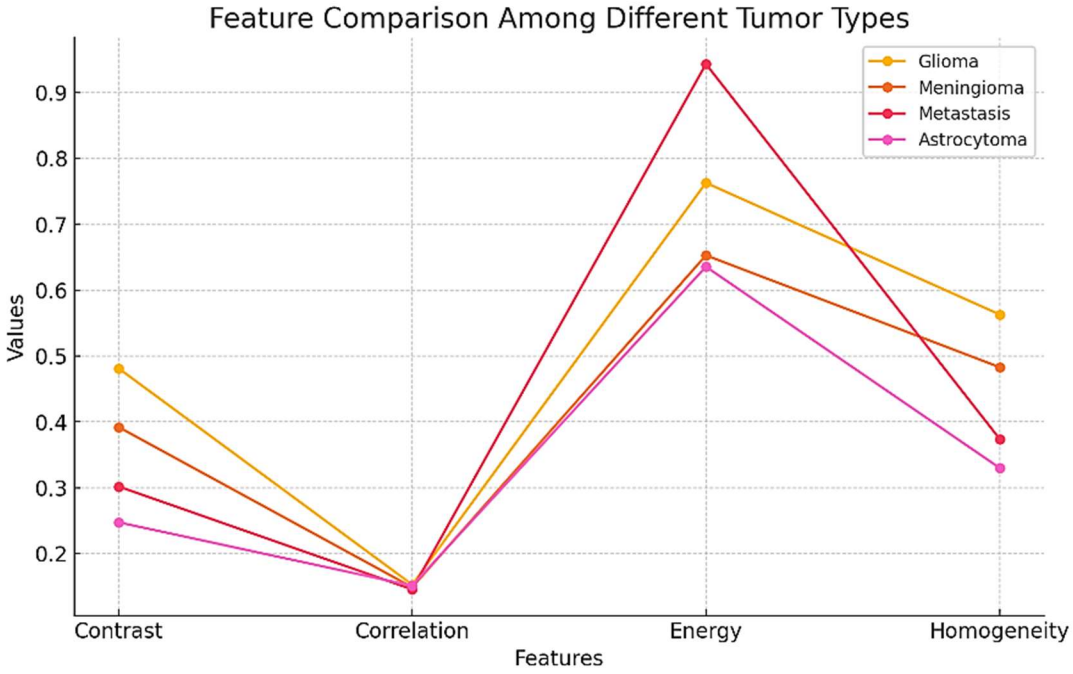


*Figure 9: Feature comparison plot among different tumor types*

### 4.2 Dataset Distribution

The BRATS dataset has been systematically classified into numerous categories of brain tumors, such as Glioma, Meningioma, Metastasis, and Astrocytoma, in order to provide a thorough assessment of the model across diverse tumor types. The categories are subdivided into training, validation, and testing subsets, guaranteeing an equitable distribution of images. A total of 1241 photos are included, with 70% designated for training, 15% for validation, and 15% for testing.

There is a total of 420 images in the Glioma category. Gliomas are neoplasms that develop in the brain and spinal cord, arising from glial cells. They are renowned for their combative disposition and can exhibit substantial variations in their conduct and reaction to therapy. In order to optimize the model training process, 294 photos, which accounts for 70% of the total, are assigned to the training set. The remaining photographs are divided evenly between the validation and testing sets, with 63 images in each set, which accounts for 15% of the total number of images. This enables the model to acquire knowledge from a significant amount of training images while being assessed on an ample amount of validation and testing data to ensure its resilience and ability to apply to various scenarios.

The Meningioma category consists of a total of 311 photos. Meningiomas are generally noncancerous growths that originate from the meninges. Gliomas are the predominant form of brain tumor and exhibit significant variability in

terms of size and symptoms. Using a proportionate distribution, 70% of the total number of photos, which is 218 images, are allocated for training. The validation set consists of 47 images, while the testing set consists of 46 images. Each set accounts for 15% of the overall dataset. This partitioning guarantees that the model is trained on a varied and inclusive collection of images, while the validation and testing sets offer a thorough evaluation.

There is a total of 260 images in the Metastasis category. Metastatic brain cancers arise when cancer cells originating from a different location in the body migrate and establish themselves in the brain. These tumors frequently occur in several sites inside the brain, posing distinct obstacles for detection and therapy. Out of the total number, 182 images (70%) are assigned for training, 39 images (15%) are allocated for validation, and another 39 images (15%) are set aside for testing. This systematic allocation enables efficient training, rigorous validation, and comprehensive testing of the model, hence guaranteeing its precision in detecting and categorizing Metastasis tumors.

There is a total of 250 photos in the Astrocytoma category. Astrocytoma arise from astrocytes, a specific type of glial cell found in the brain. They can vary in severity, ranging from low-grade, indolent tumors to high-grade, rapidly progressing ones. Gliomas are a prevalent form of brain tumor that can occur in both children and adults. The approach to treating gliomas depends on their grade. In order to preserve equilibrium, 175 photos (70%) are allocated to the training set, 38 images (15%) to the validation set, and 37 images (15%) to the testing set. This distribution guarantees that the model is provided with a comprehensive training set and sufficient validation and testing sets to appropriately assess its performance.

*Table 3: Overall Data Split for BRATS Dataset*

| Tumor Category | Training Images | Validation Images | Testing Images | Total Images |
|---|---|---|---|---|
| Glioma | 294 | 63 | 63 | 420 |
| Meningioma | 218 | 47 | 46 | 311 |
| Metastasis | 182 | 39 | 39 | 260 |
| Astrocytoma | 175 | 38 | 37 | 250 |
| **Total** | **869** | **187** | **185** | **1241** |

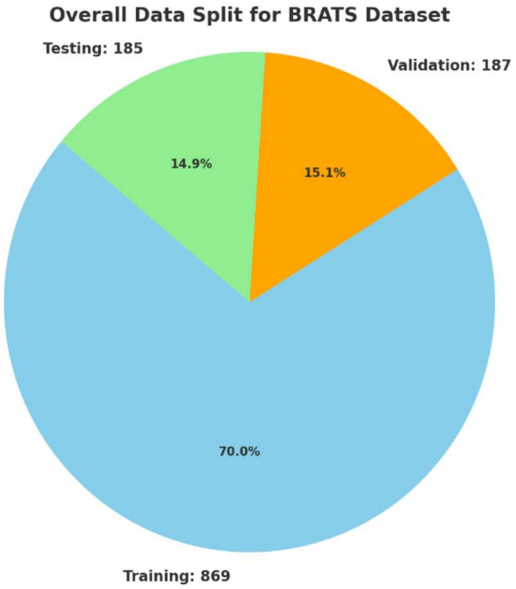


*Figure 10: Pie Chart of Data Split*

The dataset split is provided in a systematic manner as shown in Table 3 and Fig. 10 to ensure that each tumor category is sufficiently represented in each subset. This approach enables thorough training, validation, and testing of the model on various brain tumor types, thereby improving the model's accuracy, resilience, and ability to be applied to other cases. By ensuring an equitable distribution of data for every step of the model development process, the model may efficiently acquire knowledge about the unique characteristics of each tumor type and achieve high accuracy when applied to new, unknown data.

Figure 11 displays the confusion matrix, which offers a comprehensive study of the model's predictions compared to the actual classifications. It is an essential tool for assessing the performance of the model by comparing the projected classifications with the actual findings. The confusion matrix facilitates the comprehension of the model's accuracy, sensitivity, and specificity.

Figure 12 depicts the ROC (Receiver Operating Characteristic) plot, which showcases the model's capacity to differentiate between different classes. The plot displays the sensitivity (true

positive rate) vs the fall-out (false positive rate), offering valuable information.

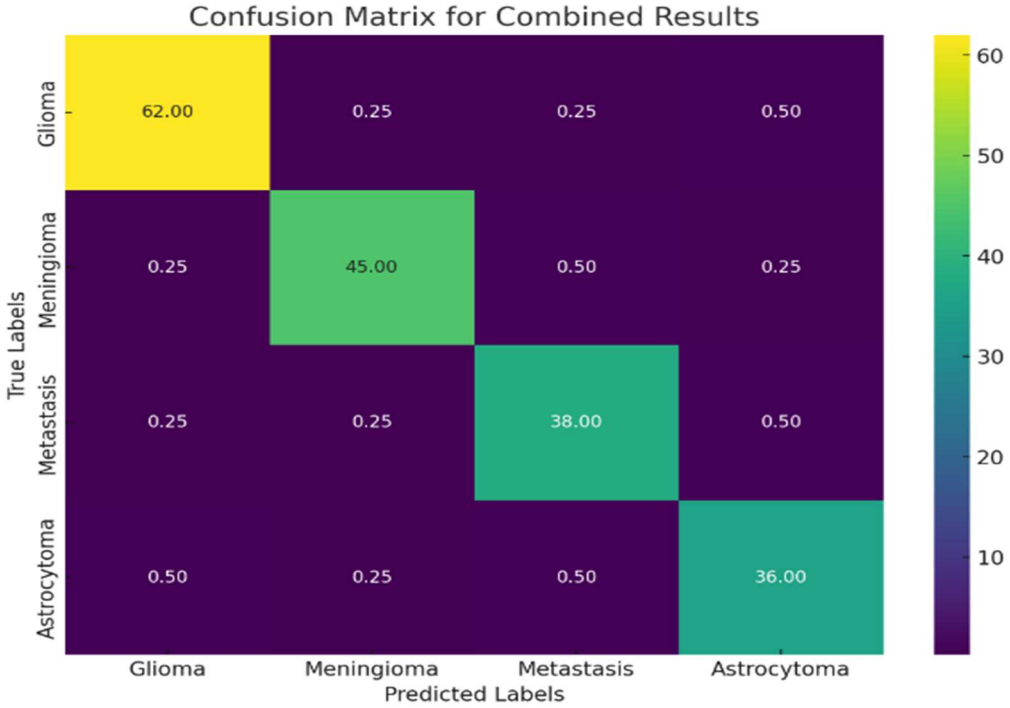


*Figure 11: Confusion Matrix*

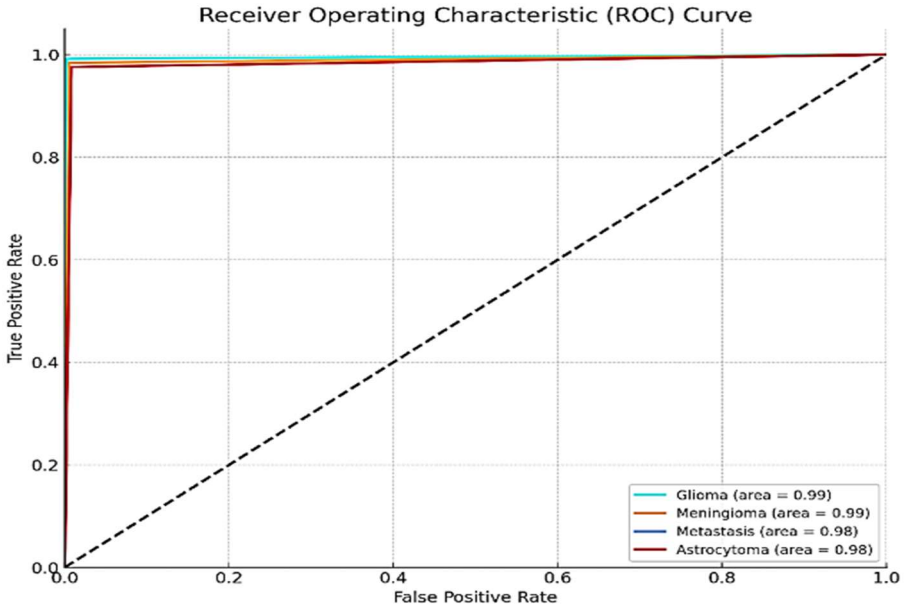


*Figure 12: ROC plot*

### 4.3 Metrics for Assessment

Table 4 presents the accuracy values of several models together with their corresponding citation numbers. The suggested model obtains a precision rate of 99.42%, surpassing previous models such as EfficientNets (98.86%), Capsule Networks (CapsNet) + VGG19 (99%), and AlexNet + GoogleNet Ensemble (99.45%). Figure 13

presents a visual representation of the accuracy comparison of the models, emphasizing the superior accuracy produced by the suggested model. This comparison illustrates the efficacy of the suggested model in precisely categorizing brain tumors.

*Table 4: Accuracy*

| Model and Citation Number | Accuracy Value |
|---|---|
| EfficientNets [21] | 98.86% |
| Capsule Networks (CapsNet) + VGG19 [22] | 99% |
| AlexNet + GoogleNet Ensemble [24] | 99.45% |
| CNN + Deer Hunting Optimization [25] | 0.917 |
| Recurrent Networks + CNN (ConvNets) [26] | 98.3% |
| Proposed Model | 99.42 % |

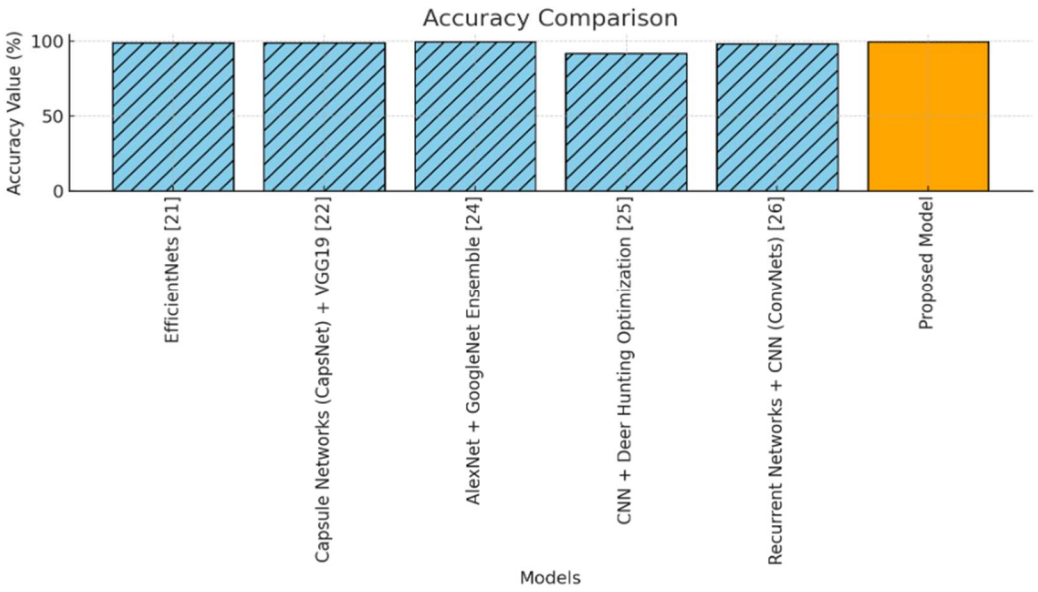


*Figure 13: Accuracy comparison plot*

*Table 5: Specificity*

| Model and Citation Number | Specificity Value |
|---|---|
| Sequential CNN [20] | 97% |
| Capsule Networks (CapsNet) + VGG19 [22] | 99% |
| CRF-RNN [23] | 93.8% |
| AlexNet + GoogleNet Ensemble [24] | 99.58% |
| CNN + Deer Hunting Optimization [25] | 91.9 % |
| Proposed Model | 99.62 % |

Table 5 displays the specificity values of several models, with the proposed model obtaining a specificity rate of 99.62%. Additional models in the study include of Sequential CNN with an accuracy of 97%, Capsule Networks (CapsNet) combined with VGG19 achieving 99% accuracy, and an ensemble of AlexNet and GoogleNet with an accuracy of 99.58%. The specificity comparison plot depicted in Figure 14 demonstrates the better specificity of the proposed model, highlighting its efficacy in accurately identifying negative situations and minimizing false positives.

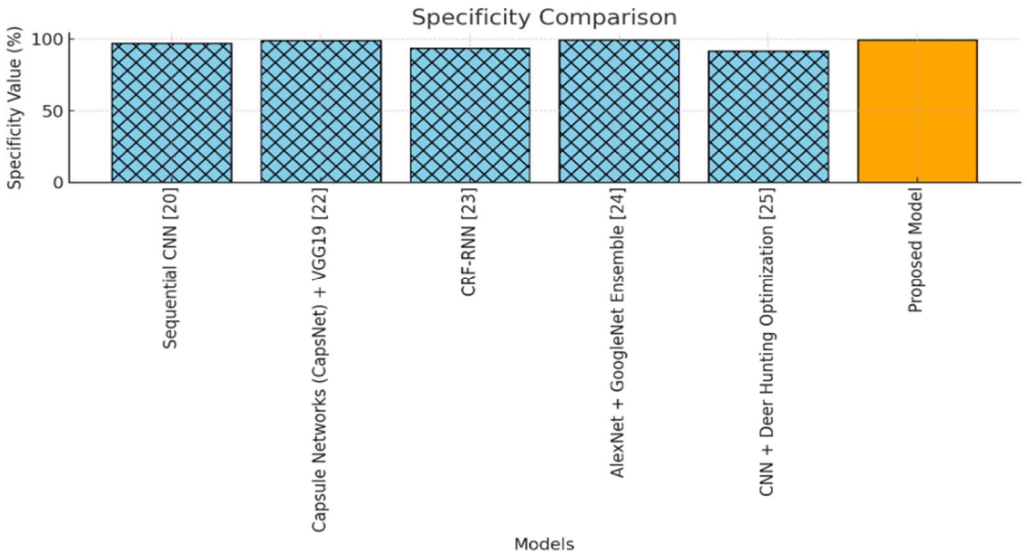


*Figure 14: Specificity comparison plot*

*Table 6: Sensitivity*

| Model and Citation Number | Specificity Value |
|---|---|
| Sequential CNN [20] | 97% |
| Capsule Networks (CapsNet) + VGG19 [22] | 99% |
| CRF-RNN [23] | 93.8% |
| AlexNet + GoogleNet Ensemble [24] | 99.58% |
| CNN + Deer Hunting Optimization [25] | 91.9 % |
| Proposed Model | 99.62 % |

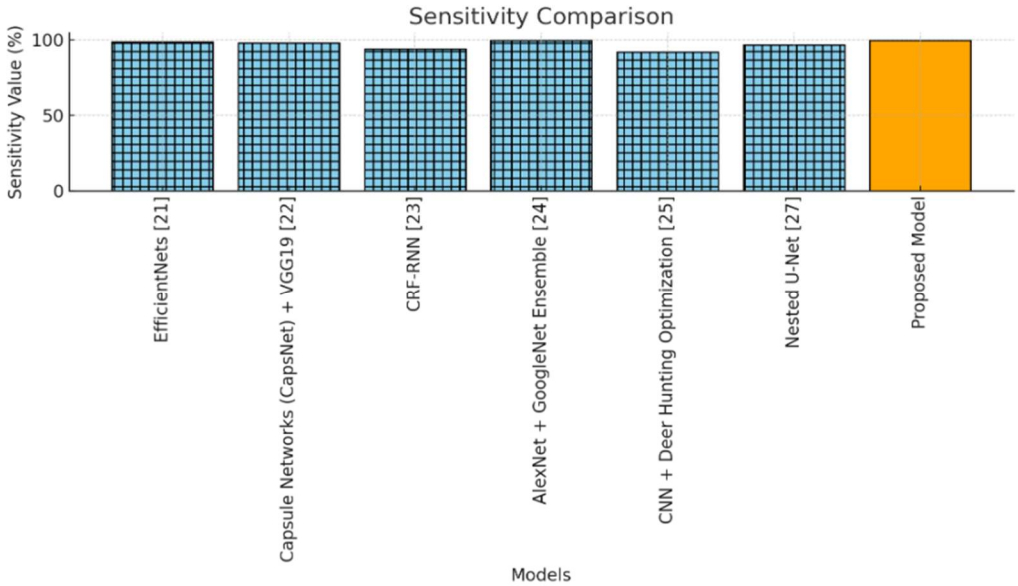


*Figure 15: Sensitivity comparison plot*

Table 6 displays the sensitivity values of different models, while the proposed model demonstrates a sensitivity of 99.81%. Additional models mentioned are EfficientNets with an

accuracy of 98.77%, Capsule Networks (CapsNet) combined with VGG19 achieving 98% accuracy, and an ensemble of AlexNet and GoogleNet with a remarkable accuracy of 99.75%. Figure 15 visually illustrates the significant sensitivity of the suggested model through a comparison plot. The model's high sensitivity ensures accurate identification of positive cases, avoiding false negatives and enabling reliable detection of brain tumors.

## 5. CONCLUSION

The proposed methodology for brain tumor classification using the BRATS dataset represents a significant advancement in the integration of sophisticated image processing and machine learning techniques. By carefully pre-processing images through spline interpolation, luminosity-based grayscale conversion, Total Variation denoising, and DBSCAN segmentation, the approach successfully preserves critical structural information while minimizing noise. The use of Haralick descriptors for feature extraction combined with t-SNE for dimensionality reduction further refines the data, enabling more precise classification. The LiquiCon-Net model, which innovatively merges ResNet-50 with Liquid Time-Constant Networks, demonstrates outstanding results, achieving accuracy, specificity, and sensitivity all exceeding 99%, surpassing many existing state-of-the-art models. While these findings are impressive and indicate strong potential for clinical application, several considerations warrant further attention. First, the model's performance on the BRATS dataset, though promising, may not fully capture the variability and complexity of real-world clinical data, which often includes diverse imaging protocols and patient demographics. Additionally, the computational complexity and training time of the LiquiCon-Net could pose challenges for widespread adoption, particularly in resource-limited settings. Future research should focus on validating this methodology across multi-center datasets and exploring ways to optimize the model for faster, more efficient deployment. In my opinion, the study marks a meaningful step forward in brain tumor classification, blending advanced feature engineering with innovative neural network architectures. However, practical translation into clinical workflows will require rigorous external validation and consideration of usability factors. With these steps, such high-precision tools could revolutionize diagnostic accuracy and treatment planning, ultimately improving patient outcomes.

## ACKNOWLEDGEMENT

This work was carried out as part of a Post-Doctoral Research (Remote) at the Singapore Institute of Technology (SIT), Singapore. The author sincerely thanks to Dr. Tan Kuan Tak and Dr. Pravin Ramdas Kshirsagar for his continuous support and valuable suggestions, which greatly improved this work. The authors also acknowledge thanks to the Singapore Institute of Technology (SIT), Singapore for doing this Post-Doctoral Research (Remote).

## REFERENCES:

[1] S. S. Spencer, W. H. Theodore, and S. F. Berkovic, "Clinical applications: MRI, SPECT, and PET," *Magnetic Resonance Imaging*, Vol. 13, No. 8, 1995, pp. 1119–1124.

[2] I. E. Naqa and M. J. Murphy, "What is machine learning?," in *Springer eBooks*, 2015, pp. 3–11.

[3] W. Tan, W. Thitøn, P. Xiang, and H. Zhou, "Multi-modal brain image fusion based on multi-level edge-preserving filtering," *Biomedical Signal Processing and Control*, Vol. 64, 2020, p. 102280.

[4] "Key statistics for brain and spinal cord tumors," American Cancer Society. [Online]. Available: https://www.cancer.org/cancer/types/brain-spinal-cord-tumors-adults/about/key-statistics.html

[5] W. Ayadi, W. Elhamzi, I. Charfi, and M. Atri, "Deep CNN for brain tumor classification," *Neural Processing Letters*, Vol. 53, No. 1, 2021, pp. 671–700.

[6] D. Rammurthy and P. K. Mahesh, "Whale Harris hawks optimization based deep learning classifier for brain tumor detection using MRI images," *Journal of King Saud University-Computer and Information Sciences*, Vol. 34, No. 6, 2020, pp. 3259–3272.

[7] S. A. Y. Al-Galal, I. F. T. Alshaikhli, and M. M. Abdulrazzaq, "MRI brain tumor medical images analysis using deep learning techniques: a systematic review," *Health and Technology*, Vol. 11, No. 2, 2021, pp. 267–282.

[8] G. S. Tandel, A. Balestrieri, T. Jujaray, N. N. Khanna, L. Saba, and J. S. Suri, "Multiclass magnetic resonance imaging brain tumor classification using artificial intelligence paradigm," *Computers in Biology and Medicine*, Vol. 122, 2020, p. 103804.

[9] R. Guerrero, C. Qin, O. Oktay, C. Bowles, L. Chen, R. Joules, R. Wolz, M. C. Valdés-Hernández, D. A. Dickie, J. Wardlaw, and D.

Rueckert, "White matter hyperintensity and stroke lesion segmentation and differentiation using convolutional neural networks," *NeuroImage Clinical*, Vol. 17, 2017, pp. 918–934.

[10] P. K. Ramtekkar, A. Pandey, and M. K. Pawar, "Innovative brain tumor detection using optimized deep learning techniques," *International Journal of Systems Assurance Engineering and Management*, Vol. 14, No. 1, 2023, pp. 459–473.

[11] S. Ruan, S. Lebonvallet, A. Merabet and J. -m. Constans, "Tumor Segmentation From A Multispectral Mri Images By Using Support Vector Machine Classification," *2007 4th IEEE International Symposium on Biomedical Imaging: From Nano to Macro, Arlington, VA, USA*, 2007, pp. 1236-1239.

[12] M. F. Rabbi, S. M. Mahedy Hasan, A. I. Champa, M. AsifZaman and M. K. Hasan, "Prediction of Liver Disorders using Machine Learning Algorithms: A Comparative Study," *2020 2nd International Conference on Advanced Information and Communication Technology (ICAICT), Dhaka, Bangladesh*, 2020, pp. 111-116.

[13] K. Munir, F. Frezza, and A. Rizzi, "Brain tumor segmentation using 2D-UNET Convolutional Neural Network," *in Studies in computational intelligence*, 2020, pp. 239–248.

[14] D. Zhang, G. Huang, Q. Zhang, J. Han, J. Han, and Y. Yu, "Cross-modality deep feature learning for brain tumor segmentation," *Pattern Recognition*, Vol. 110, 2020, p. 107562.

[15] D. Konar, S. Bhattacharyya, S. Dey, and B. K. Panigrahi, "Opti-QIBDS NET: a Quantum-Inspired optimized Bi-Directional self-supervised neural network architecture for automatic brain MR image segmentation," *TENCON 2021 - 2021 IEEE Region 10 Conference (TENCON)*, 2019, pp. 761–766.

[16] N. Kesav and M. G. Jibukumar, "Efficient and low complex architecture for detection and classification of Brain Tumor using RCNN with Two Channel CNN," *Journal of King Saud University - Computer and Information Sciences*, Vol. 34, No. 8, 2021, pp. 6229–6242.

[17] M. Nazir, S. Shakil, and K. Khurshid, "Role of deep learning in brain tumor detection and classification (2015 to 2020): A review," *Computerized Medical Imaging and Graphics*, Vol. 91, 2021, p. 101940.

[18] B. H. Menze, A. Jakab, S. Bauer, J. Kalpathy-Cramer, K. Farahani, J. Kirby, Y. Burren, N. Porz, J. Slotboom, R. Wiest, L. Lanczi, E. Gerstner, M.-A. Weber, T. Arbel, B. B. Avants, N. Ayache, P. Buendia, D. L. Collins, N. Cordier, J. J. Corso, A. Criminisi, T. Das, H. Delingette, C. Demiralp, C. R. Durst, M. Dojat, S. Doyle, J. Festa, F. Forbes, E. Geremia, B. Glocker, P. Golland, X. Guo, A. Hamamci, K. M. Iftekharuddin, R. Jena, N. M. John, E. Konukoglu, D. Lashkari, J. A. Mariz, R. Meier, S. Pereira, D. Precup, S. J. Price, T. R. Raviv, S. M. S. Reza, M. Ryan, D. Sarikaya, L. Schwartz, H.-C. Shin, J. Shotton, C. A. Silva, N. Sousa, N. K. Subbanna, G. Szekely, T. J. Taylor, O. M. Thomas, N. J. Tustison, G. Unal, F. Vasseur, M. Wintermark, D. H. Ye, L. Zhao, B. Zhao, D. Zikic, M. Prastawa, M. Reyes, and K. Van Leemput, "The Multimodal Brain Tumor Image Segmentation Benchmark (BRATS)," *IEEE Transactions on Medical Imaging*, Vol. 34, No. 10, 2014, pp. 1993–2024.

[19] B. T. Ahmed, "Lung Cancer prediction and detection using Image Processing Mechanisms: An Overview," *Signal and Image Processing Letters*, Vol. 1, No. 3, 2019.

[20] A. Alshuhail, A. Thakur, R. Chandramma, T. R. Mahesh, A. Almusharraf, V. V. Kumar, and S. B. Khan, "Refining neural network algorithms for accurate brain tumor classification in MRI imagery," *BMC Medical Imaging*, Vol. 24, No. 1, 2024.

[21] F. Zulfiqar, U. I. Bajwa, and Y. Mehmood, "Multi-class classification of brain tumor types from MR images using EfficientNets," *Biomedical Signal Processing and Control*, Vol. 84, 2023, p. 104777.

[22] A. Jabbar, S. Naseem, T. Mahmood, T. Saba, F. S. Alamri, and A. Rehman, "Brain tumor Detection and Multi-Grade segmentation through hybrid CAPS-VGGNET model," IEEE Access, Vol. 11, 2023, pp. 72518–72536.

[23] G. M, P. L. K, S. R. Arumugam, and S. N, "Conditional random field-recurrent neural network segmentation with optimized deep learning for brain tumour classification using magnetic resonance imaging," *The Imaging Science Journal*, Vol. 71, No. 3, 2023, pp. 199–220.

[24] C. Swarup, K. U. Singh, A. Kumar, S. K. Pandey, N. Varshney, and T. Singh, "Brain tumor detection using CNN, AlexNet & GoogLeNet ensembling learning approaches," *Electronic Research Archive*, Vol. 31, No. 5, 2023, pp. 2900–2924.

[25] P. Kanchanamala, R. KG, and M. B. J. Ananth, "Optimization-enabled hybrid deep learning for brain tumor detection and classification from MRI," *Biomedical Signal Processing and Control*, Vol. 84, 2023, p. 104955.

[26] A. K. Sharma, S. Tiwari, G. Aggarwal, N. Goenka, A. Kumar, P. Chakrabarti, T. Chakrabarti, R. Gono, Z. Leonowicz, and M. Jasinski, "Dermatologist-Level classification of skin cancer using cascaded ensembling of convolutional neural network and handcrafted features based deep neural network," *IEEE Access*, Vol. 10, 2022, pp. 17920–17932.

[27] C. Mathews, and A. Mohamed, "Nested U-Net with Enhanced Attention Gate and Compound Loss for Semantic Segmentation of Brain Tumor from Multimodal MRI," International Journal of Intelligent Engineering and Systems, Vol. 15, No. 4, 2022.